

Dynamics of Competitive Polymer Adsorption onto Planar Surfaces in Good Solvent

Niklas Källrot and Per Linse*

Physical Chemistry, Center for Chemistry and Chemical Engineering, Lund University,
P.O. Box 124, S-221 00 Lund, Sweden

Received: September 8, 2009; Revised Manuscript Received: January 28, 2010

Adsorption of mixed polymer solutions in good solvent containing polymers of different chain length has been studied by applying simulation techniques on a coarse-grained bead–spring polymer model. Fully flexible polymers at varying bead–surface interaction strength and different combinations of flexible, semiflexible, and stiff polymers at a single bead–surface interaction strength have been examined. Monte Carlo simulation techniques have been employed to investigate static equilibrium properties and Brownian dynamic simulations to follow the dynamics of the adsorption process. The properties examined comprise the adsorbed number of polymers, adsorbed number of beads, bead density profiles, components of the polymer radius of gyration, tail, loop, and train configurations, and nematic bond order of adsorbed beads. The adsorption involves an initially independent adsorption of the two polymer types followed by competitive adsorption. The competitive adsorption is characterized by a maximum of the adsorbed amount and a desorption of the polymer with the smallest surface affinity and a continued, but reduced, growth of the adsorbed amount of the polymer with the largest surface affinity. The surface affinity difference between the two polymer types of different length increased with increasing bead–surface interaction. Furthermore, the surface affinity of a polymer initially decreased but then largely increased at increasing stiffness. As a consequence, a stiff short polymer was found to displace a 4-fold longer flexible polymer. The spatial extension of adsorbed polymers as characterized by the radius of gyration parallel and perpendicular to the surface of a polymer of a given flexibility was independent of the flexibility of the other polymer type. The fraction of beads in tails was increased and in trains reduced as the surface affinity of the dissimilar polymer type was raised. Finally, the adsorption layer of a stiff polymer possesses a nematic bond order. In mixed polymer systems, the nematic bond order of a given polymer type manifests a dependence on the flexibility of the other type.

1. Introduction

Adsorption of polymers from solution onto solid surfaces has been studied extensively for a long time^{1,2} due to the applicability in a vast number of technological aspects.³ The intrinsic structural degrees of conformational freedom associated with polymers affects adsorption both in terms of equilibrium adsorbed structures and the preceding dynamics of the adsorption process. In the vicinity of an adsorbing surface, increased density of polymers along with conformational changes associated with the adsorption gives rise to slower dynamics. These features influence the adsorption rates and the exchange rates of polymers. Specifically, competitive adsorption and exchange of polymers differing in length or intrinsic stiffness is affected. The nature of competitive adsorption onto solid surfaces has been studied both experimentally^{4–10} and theoretically.^{11–16}

Kinetics of competitive adsorption has examined for homopolymers of differing molecular weight by adsorbing polyethylene oxide (PEO) and polystyrene (PS) onto silica wafers.^{4,5,7} Experimental studies have also been conducted on adsorption of mixed solutions with varying degree of polymer flexibility.^{4,8,10} In a simple yet clever experimental setup, a polysaccharide (pullulan) in competitive adsorption with its carboxylated analogue was used to induce and ascertain *trapped* nonadsorbing polymers at a surface. Furthermore, Postmus et al.⁹ have considered competitive adsorption between nonionic surfactant and nonionic polymers relating the decrease in adsorption kinetics and the existence of a critical molar mass with a shift in the critical surface association concentration (CSAC). The

latter phenomena were subsequently modeled using a self-consistent field approach,¹⁶ which qualitatively captured the general physical behavior of the experimental system. In a recent study, Chornaya et al.⁸ have investigated the kinetics of the competitive adsorption of flexible PBMA and stiff CTA polymers onto Aerosil at different bulk concentrations. They were able to show an initial increase in coverage by the flexible polymers, followed by a desorption of these as the coverage of stiff polymers was increased at later times.

Several theories have been developed to predict adsorption fractionation of polydisperse mixtures.^{11,12} Kinetic theories of polydisperse mixtures which focused on competitive adsorption and exchange have been presented, starting either from a preadsorbed layer which gradually becomes replaced¹⁵ or from an uncovered surface in contact with a mixed polymer solution.¹³ Furthermore, a dynamic approach using lattice Monte Carlo simulations has been made,¹⁴ where the general behavior of the displacement of adsorbed shorter by longer polymers at a surface was captured by monitoring the evolution of the train segment density.

In previous contributions by Källrot et al., we have examined time dependent properties during the adsorption of homopolymers in good solvent by Brownian dynamics. Starting with single polymer systems with varying bead–surface interaction strength and intrinsic stiffness of the polymer, Källrot and Linse¹⁷ identified three distinct phases of the adsorption process involving (i) a distortion phase, (ii) an attachment phase, and (iii) a relaxation phase. In our second contribution,¹⁸ adsorption of flexible homopolymers in solution onto planar surfaces was

investigated with respect to polymer length and solution density. Here, we found an additional process associated with the relaxation of the number of adsorbed polymers at the surface. In a third paper,¹⁹ we investigated the adsorption of polymers from solution at varying bead–surface interaction strength and polymer flexibility. We observed yet a slower relaxation mechanism involving a nematic bond order formation among adsorbed rod-like polymers. Furthermore, averaged adsorption times and time needed for polymers to become fully integrated in the adsorbed layer were considered.

In this work, we examine the adsorption dynamics of mixed polymer systems at a polymer length ratio of 4 with (i) varying bead–surface interaction strength for flexible polymers and (ii) various combinations of intrinsic stiffness of the two polymer types at a fixed bead–surface interaction strength. The investigations were conducted using a coarse-grained bead–spring model, employing Brownian and Monte Carlo simulation techniques.

2. Model

The model used in this work is to a large extent based on a coarse-grained model previously employed for polymer adsorption from a monodisperse polymer solution.^{17–19} Briefly, a polymer is composed of spherical beads connected via harmonic bonds, and its stiffness is regulated by a harmonic angular potential. The mixed polymer solution is composed of $N_{p,s}$ short polymers consisting of $N_{b,s}$ spherical beads and of $N_{p,l}$ long polymers consisting of $N_{b,l}$ spherical beads. The total number of beads N is thus given by the sum of the two polymer lengths, $N = \sum_{\gamma} N_{p,\gamma} N_{b,\gamma}$, where $\gamma = \{s, l\}$ (short and long).

The mixed polymer solution was confined within a rectangular simulation box with the box lengths L_x , L_y , and L_z . Adsorbing surfaces were invoked at $z = \pm(L_z/2)$, whereas in the x - and y -directions periodic boundary conditions were applied. The length of the box was set to $L_x = L_y = 200$ Å and $L_z = 240$ Å. Furthermore, due to the symmetry of the simulation box along the z -axis, results are averaged over both surfaces, and we shall from here on only refer to events occurring at a single surface unless otherwise stated. In the following, a coordinate system where the z -axis starts at $z = \pm(L_z/2)$ with its direction pointing into the solution is adopted.

We express the total energy U for the system as a sum of four different terms: nonbonded bead–bead potential energy U_{nonbond} , bond potential energy U_{bond} , angular potential energy U_{angle} , and a bead–surface potential energy U_{surf} , according to

$$U = U_{\text{nonbond}} + U_{\text{bond}} + U_{\text{angle}} + U_{\text{surf}} \quad (1)$$

The nonbonded bead–bead potential energy is assumed to be pairwise additive according to

$$U_{\text{nonbond}} = \sum_{i < j}^N u(r_{ij}) \quad (2)$$

where the interaction between beads i and j at a distance r_{ij} between them is described by a truncated and shifted repulsive Lennard-Jones (LJ) potential energy

$$u(r_{ij}) = \begin{cases} 4\varepsilon \left[-\left(\frac{\sigma}{r_{ij}}\right)^6 + \left(\frac{\sigma}{r_{ij}}\right)^{12} + \frac{1}{4} \right], & r_{ij} \leq 2^{1/6}\sigma \\ 0, & r_{ij} > 2^{1/6}\sigma \end{cases} \quad (3)$$

where $\sigma = 3.405$ Å is the diameter of the bead and $\varepsilon = 0.9961$ kJ/mol the interaction strength. The truncation and the shift of the Lennard-Jones potential yield as soft repulsive potential between interacting beads.

The bond and angular potential energies are composed of simple harmonic functions, given by

$$U_{\text{bond}} = \frac{1}{2}k_{\text{bond}} \sum_{p=1}^{N_{p,\gamma}} \sum_{i=1}^{N_{b,\gamma}-1} (r_{i,p} - r_{\text{eq}})^2 \quad (4)$$

$$U_{\text{angle}} = \frac{1}{2}k_{\text{angle}} \sum_{p=1}^{N_{p,\gamma}} \sum_{i=2}^{N_{b,\gamma}-1} (\theta_{i,p} - \theta_{\text{eq}})^2 \quad (5)$$

where $k_{\text{bond}} = 2.4088$ kJ/mol is the bond force constant and k_{angle} the angular force constant which regulates the stiffness of the chains. Furthermore, $r_{\text{eq}} = 5.0$ Å is the equilibrium bond length and $\theta_{\text{eq}} = 180^\circ$ the equilibrium bond angle. In the presence of all interactions, the root-mean-square bead–bead separation of bonded beads becomes $\langle R_{\text{bb}}^2 \rangle^{1/2} \approx 5.6$ Å.

The polymer–surface interaction is taken as a sum of bead–surface interactions according to

$$U_{\text{surf}} = \sum_{i=1}^N (u_{\text{surf}}(z_i) + u_{\text{surf}}(L_z - z_i)) \quad (6)$$

where an attractive 3–9 LJ potential²⁰

$$u_{\text{surf}}(z_i) = \frac{2\pi}{3} \rho_s \sigma_s^3 \varepsilon_s \left[-\left(\frac{\sigma_s}{z_i}\right)^3 + \frac{2}{15} \left(\frac{\sigma_s}{z_i}\right)^9 \right] \quad (7)$$

is used for the interaction between bead i and the surface in the adsorption simulations. In eq 7, ρ_s is the density of the (hypothetical) particles forming the surface, σ_s the mean diameter of beads and surface particles, ε_s a potential energy parameter describing the bead–surface interaction, and z_i the z -coordinate of bead i with respect to the surface. For simplicity, $\sigma_s = 3.5$ Å and $\rho_s \sigma_s^3 = 1$ were chosen. With this attractive 3–9 LJ potential, the potential minimum appears at $z_{\min} = (2/5)^{1/6} \sigma_s \approx 3.0$ Å and amounts to $u_{\text{surf}}(z_{\min}) = -[2\pi(10)^{1/2}/9]\rho_s \sigma_s^3 \varepsilon_s \approx -2.2\varepsilon_s$.

The intrinsic stiffness of the polymers was characterized by calculating the persistence length based on the local folding l_p of a single polymer at infinite dilution according to $l_p = \langle R_{\text{bb}}^2 \rangle^{1/2}/(1 + \langle \cos \theta \rangle)$.²¹ Further data describing the model systems are collected in Table 1.

The solutions that were studied in this work consisted of a mixture of polymers of chain length $N_{b,s} = 20$ and $N_{b,l} = 80$. The polymer solutions contained $N_{p,s} = 94$ short and $N_{p,l} = 80$ long polymers, which gives a density close to the common overlap density obtained by utilizing the radius of gyration at infinite dilution. The parameters varied in this work are (i) the adsorption strength of the adsorbing surface (ε_s) and (ii) the angular force constant (k_{angle}).

TABLE 1: Model Parameters

box length (x , y-dir)	$L_x = L_y = 200 \text{ \AA}$
box length (z -dir)	$L_z = 240 \text{ \AA}$
temperature	$T = 298 \text{ K}$
number of polymers	$N_{p,s} = 94$ and $N_{p,l} = 80$
number of beads in a chain	$N_{b,s} = 20$ and $N_{b,l} = 80$
bead-bead LJ parameter	$\sigma = 3.405 \text{ \AA}$
bead-bead LJ parameter	$\epsilon = 0.9961 \text{ kJ/mol}$
force constant of bond potential	$k_{\text{bond}} = 2.4088 \text{ kJ/mol}$
force constant of angle potential	$k_{\text{angle}} = 0, 1.2, \text{ and } 10 \text{ J/(mol deg}^2)$
equilibrium separation of bond potential	$r_{\text{eq}} = 5.0 \text{ \AA}$
equilibrium angle of angle potential	$\theta_{\text{eq}} = 180^\circ$
bead-surface LJ parameter	$\sigma_s = 3.5 \text{ \AA}$
bead-surface LJ parameter	$\epsilon_s = 1.5, 2.0, 2.5, \text{ and } 3.0 \text{ kJ/mol}$

TABLE 2: Specifications of Investigated Systems

set I ^a		set II ^b		set III ^b	
ϵ_s , kJ/mol	$u_{\text{surf}}(z_{\min})$, kJ/mol	k_{angle} , J/(mol deg ²)	label ^c	k_{angle} , J/(mol deg ²)	label ^d
1.5	3.312	0/0 ^e	f/f	0/0 ^e	f/f
2.0	4.415	10/0	s/f	1.2/0	sf/f
2.5 ^e	5.519	0/10	f/s	0/1.2	f/sf
3.0	6.623	10/10	s/s	1.2/1.2	st/sf

^a $k_{\text{angle}} = 0 \text{ J/mol deg}^2$. ^b $\epsilon_s = 2.5 \text{ kJ/mol}$. ^c f = flexible and s = stiff. ^d f = flexible and sf = semiflexible. ^e Same system, also referred to as the reference system.

The investigated systems are divided into three sets. In set I, $\epsilon_s = 1.5, 2.0, 2.5, \text{ and } 3.0 \text{ kJ/mol}$ with both polymer types modeled as fully flexible ($k_{\text{angle}} = 0 \text{ J/(mol deg}^2)$). This mixed polymer solution will be referred to as a *bidisperse* polymer solution. In set II, systems involving all four different combinations of the two polymer lengths and the two angular force constants $k_{\text{angle}} = 0$ and $10 \text{ J/(mol deg}^2)$ at $\epsilon_s = 2.5 \text{ kJ/mol}$ were considered. Finally, set III involved the smaller bending force constant of $k_{\text{angle}} = 1.2 \text{ J/(mol deg}^2)$. The persistence length of the polymers with the different angular force constants $k_{\text{angle}} = 0, 1.2, \text{ and } 10 \text{ J/(mol deg}^2)$ became $l_p \approx 7, 13, \text{ and } 77 \text{ \AA}$, respectively. Further details of the examined systems are given in Table 2. The system characterized by $\epsilon_s = 2.5 \text{ kJ/mol}$ and $k_{\text{angle}} = 0 \text{ J/(mol deg}^2)$ for both polymer types is common of the three sets, and this system is also referred to as the *reference* system.

3. Method

Both static and dynamic properties of the mixed polymer solutions have been examined. The adsorption dynamics including conformational relaxation were examined using Brownian dynamics (BD) simulations. Static equilibrium properties along with the initial preparation of the mixed solutions of the BD simulations were conducted using Monte Carlo (MC) simulations. All simulations were carried out using the canonical (*NVT*) ensemble, characterized by a constant number of particles, volume, and temperature. Despite a variation in the polymer density far from the surfaces at varying degree of adsorption, this has no influence on our interpretation of data.

The adsorption simulation studies were carried out as follows: (i) First, an equilibrated polymer solution was generated by MC simulations using a slightly smaller box to generate polymer-free zones adjacent to the adsorbing surfaces in the subsequent BD simulations. Here, we used $L_z = 200 \text{ \AA}$ with hard walls in the z -direction. (ii) Second, the hard walls were removed, the box length in the z -direction was increased to $L_z = 240 \text{ \AA}$, and

attractive surfaces, whose potential was described by eq 7, were invoked. (iii) Finally, the BD simulations were performed. Hence, the initial configurations of the BD simulations involved an $\sim 20 \text{ \AA}$ thick polymer-free zone adjacent to each surface.

In addition, complementary BD and MC simulations of corresponding bulk systems were performed to provide properties of the bulk solutions. These simulations were performed with periodic boundary conditions applied in all three directions. Naturally, in these simulations, the U_{surf} term in eq 1 was absent.

The motion of the polymer beads in the BD simulations was described by Ermak²²

$$\mathbf{r}_i(t + \Delta t) = \mathbf{r}_i(t) + \frac{D_0 \Delta t}{k_b T} \mathbf{F}_i(t) + \mathbf{R}_i(t; \Delta t) \quad (8)$$

where $\mathbf{r}_i(t + \Delta t)$ is the location of bead i at time $t + \Delta t$, $\mathbf{r}_i(t)$ the location of bead i at time t , D_0 the bead self-diffusion coefficient in the absence of systematic forces, k_b Boltzmann's constant, T the temperature, and $\mathbf{F}_i(t)$ the systematic force on bead i at time t arising from the potential energy U given by eq 1. Furthermore, $\mathbf{R}_i(t; \Delta t)$ is a random displacement of bead i representing the effect of collisions with solvent molecules at time t , and is sampled from a Gaussian distribution with the mean $\langle \mathbf{R}_i(t; \Delta t) \rangle = 0$ and the variance $\langle \mathbf{R}_i(t; \Delta t) \cdot \mathbf{R}_j(t'; \Delta t) \rangle = 6D_0 \Delta t \delta_{ij} \delta(t - t')$ as obtained from the fluctuation-dissipation theorem. In this work, hydrodynamic interactions were neglected.

A bead self-diffusion coefficient of $D_0 = 0.1 \text{ \AA}^2/\text{ps}$ was used, and an integration time step of $\Delta t = 0.025 \text{ ps}$ was employed. The BD simulations involved 2×10^8 time steps, providing a nominal simulation time of $5 \mu\text{s}$. Using $\tau_{\text{BD}} = \sigma^2/D_0 = 116 \text{ ps}$ as the conventional unit of time, the integration time step becomes $\Delta t = 2.2 \times 10^{-4} \tau_{\text{BD}}$ and the total simulation time $4.3 \times 10^4 \tau_{\text{BD}}$.

The MC simulations were performed according to the Metropolis algorithm,²³ using three types of trial moves: (i) translation of individual beads, (ii) reptation of polymers, and (iii) translation of entire polymers. The translational displacement parameter of single-bead trial moves was 3 \AA , the probability of a reptation and of a chain translation was $1/N_{b,y}$, $y = \{s, l\}$, of that of a single-bead trial move, and the chain translational displacement parameter was 5 \AA . The MC simulations comprised 1×10^5 trial moves per bead after an equilibration consisting of 1.1×10^6 trial moves per bead. All simulations were performed using the integrated Monte Carlo/molecular dynamics/Brownian dynamics simulation package MOLSIM.²⁴

The nonlocal character of some of the MC trial moves and the only local changes between successive BD time steps make the convergence of MC simulations much faster than that of BD simulations. The use of the MC simulation technique in the present study facilitates (i) equilibration, (ii) determination of static properties of equilibrium systems, and (iii) assessment of how systems starting from nonquilibrium states approach equilibrium during the BD simulation.

4. Dynamical Analysis

Several time-dependent properties were examined during the adsorption process of the polymers. The location of a polymer of type γ at a time t was described using its center of mass $\mathbf{r}_{\text{com},\gamma}(t)$ defined according to

$$\mathbf{r}_{\text{com},\gamma}(t) = \frac{1}{N_{\text{b},\gamma}} \sum_{i=1}^{N_{\text{b},\gamma}} \mathbf{r}_i(t) \quad (9)$$

where $\mathbf{r}_i(t) = [x_i(t), y_i(t), z_i(t)]$ is the coordinate of bead i at time t . Changing the notation $\mathbf{r}_i(t)$ to $z_i(t)$ in eq 9 gives the center of mass along the z -axis, $z_{\text{com},\gamma}(t)$, which is a useful measure of the position of the polymers relative to a surface.

There is a structural rearrangement of the polymers from a three-dimensional to a flatter object during the adsorption. This process was followed by studying the perpendicular (\perp) and parallel (\parallel) component of the root-mean-square radius of gyration, $\langle R_{g,\gamma}^2(t) \rangle^{1/2}$, according to

$$\langle R_{g,\gamma}^2(t) \rangle_{\perp} = \left\langle \frac{1}{N_{\text{b},\gamma}} \sum_{i=1}^{N_{\text{b},\gamma}} [z_i(t) - z_{\text{com}}(t)]^2 \right\rangle \quad (10)$$

$$\langle R_{g,\gamma}^2(t) \rangle_{\parallel} = \left\langle \frac{1}{N_{\text{b},\gamma}} \sum_{i=1}^{N_{\text{b},\gamma}} \{[x_i(t) - x_{\text{com}}(t)]^2 + [y_i(t) - y_{\text{com}}(t)]^2\} \right\rangle \quad (11)$$

satisfying $\langle R_{g,\gamma}^2(t) \rangle = \langle R_{g,\gamma}^2(t) \rangle_{\perp} + \langle R_{g,\gamma}^2(t) \rangle_{\parallel}$.

A polymer was considered as being adsorbed if at least one of its beads was in contact with a surface, here defined by $z_i < 6 \text{ \AA}$. Recall that the minimum of the bead–surface potential is located at $z_{\min} \approx 3 \text{ \AA}$. The criteria for when a polymer is considered adsorbed is somewhat arbitrary. The choice of adsorption distance will generally influence the numbers obtained but not qualitative aspects.

The structure of adsorbed polymers was described by using loop, tail, and train subchains.² A subchain of adsorbed beads is referred to as a train, a nonadsorbed subchain with both ends bonded to trains as a loop, and a nonadsorbed subchain with one end bonded to a train as a tail. The average total number of beads in subchains of type α at time t of a polymer type γ will be denoted by $\langle N_{\alpha,\gamma}(t) \rangle$, with $\alpha = \{\text{tail, loop, train}\}$. By conservation: $\sum_{\alpha} \langle N_{\alpha,\gamma}(t) \rangle = N_{\text{b},\gamma}$.

The degree of nematic order appearing in the adsorbed polymer layer was examined by considering the bond order parameter η . The degree of bond order in the proximity of the adsorbed bond i , η_i , was evaluated as

$$\eta_i = \lambda_i^+ \quad (12)$$

where λ_i^+ is the largest eigenvalue of the 3×3 matrix \mathbf{B}_i , in which the elements are defined by

$$\mathbf{B}_{\alpha\beta,i} = \frac{1}{N_{V_i,j \in V_i}} \sum' \frac{1}{2} (3\mathbf{b}_{\alpha,j} \cdot \mathbf{b}_{\beta,j} - \delta_{\alpha\beta}) \quad (13)$$

where \mathbf{b}_j is the normalized bond axis vector of bond j , $\{\alpha, \beta\} = \{x, y, z\}$, and the summation involves N_{V_i} bonds in the spherical volume V_i with the radius R_η centered at bond i . The prime on the summation symbol indicates that the sum is taken over bonds residing in polymers of the same type as the polymer in which bond i resides. Only bonds that are adsorbed are included in the sum; thus, in practice, bonds in a disk of radius R_η and height 3 \AA are considered. The bond order parameter ranges from zero for random bond directions to unity for completely parallel bond directions. Results will be given for the radius of $R_\eta = 20 \text{ \AA}$.

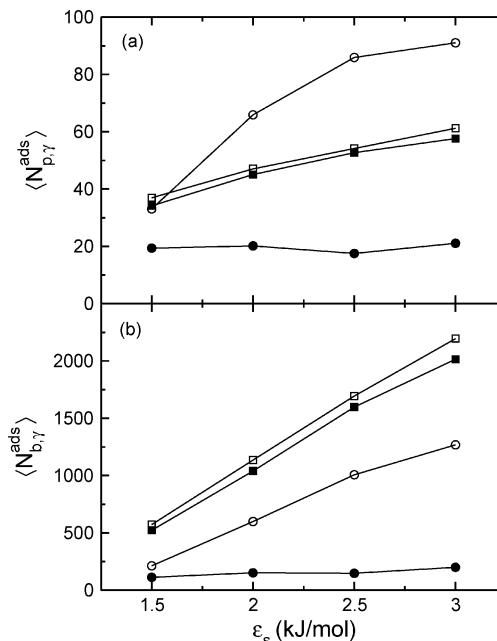


Figure 1. (a) Average number of adsorbed polymers $\langle N_{p,\gamma}^{\text{ads}} \rangle$ and (b) average number of adsorbed beads $\langle N_{b,\gamma}^{\text{ads}} \rangle$ as a function of the bead–surface parameter ϵ_s of the 20-mer (circles) and the 80-mer (squares) for bidisperse polymer systems belonging to set I (filled symbols) and for monodisperse systems (open symbols).

We will present the equilibrium probability bond order distribution $P(\eta)$ and the time-dependent bond order $\eta(t)$ of the two polymer types separately.

Simulated dynamic properties were sampled from a subset of 10^4 trajectories, evenly distributed from the start to the end of the simulation, yielding $\Delta t_{\text{samp}} = 0.5 \text{ ns}$. The properties were then averaged over exponentially increasing block lengths with the initial length of $2.5\Delta t_{\text{samp}} = 1.25 \text{ ns}$, which was then increased with a multiplicative factor of 1.5 throughout the rest of the simulation. This method of sampling data enabled us to monitor various subprocesses that occur on different time scales during the full adsorption.

The bracket notation $\langle \dots \rangle$ in eqs 9–11 and elsewhere depends on the boundary conditions and simulation method. In the MC simulations, the brackets denote an ensemble and polymer average, whereas, in the nonequilibrium BD simulations of the systems with attractive surfaces, they denote an average over adsorbed polymers.

5. Static Equilibrium Properties

In the following section, we will first consider static properties of the polymer solution in contact with the adsorbing surface at equilibrium. This will be made first for systems belonging to set I and thereafter for systems belonging to sets II and III.

5.1. Set I. Figure 1 shows the average number of adsorbed polymers $\langle N_{p,\gamma}^{\text{ads}} \rangle$, $\gamma = \{s, l\}$, and the average number of adsorbed beads $\langle N_{b,\gamma}^{\text{ads}} \rangle$, $\gamma = \{s, l\}$, as a function of the bead–surface interaction strength for systems belonging to set I. Corresponding data are also given for systems with only one polymer component at the same density as in the bidisperse polymer solution. Generally, both the number of adsorbed 80-mers and the number of adsorbed beads of the 80-mer (filled squares) (i) increase monotonically with increasing bead–surface interaction strength and (ii) are slightly less but close to corresponding numbers in the absence of the shorter 20-mer (open squares). The number of adsorbed 20-mers and the number of adsorbed

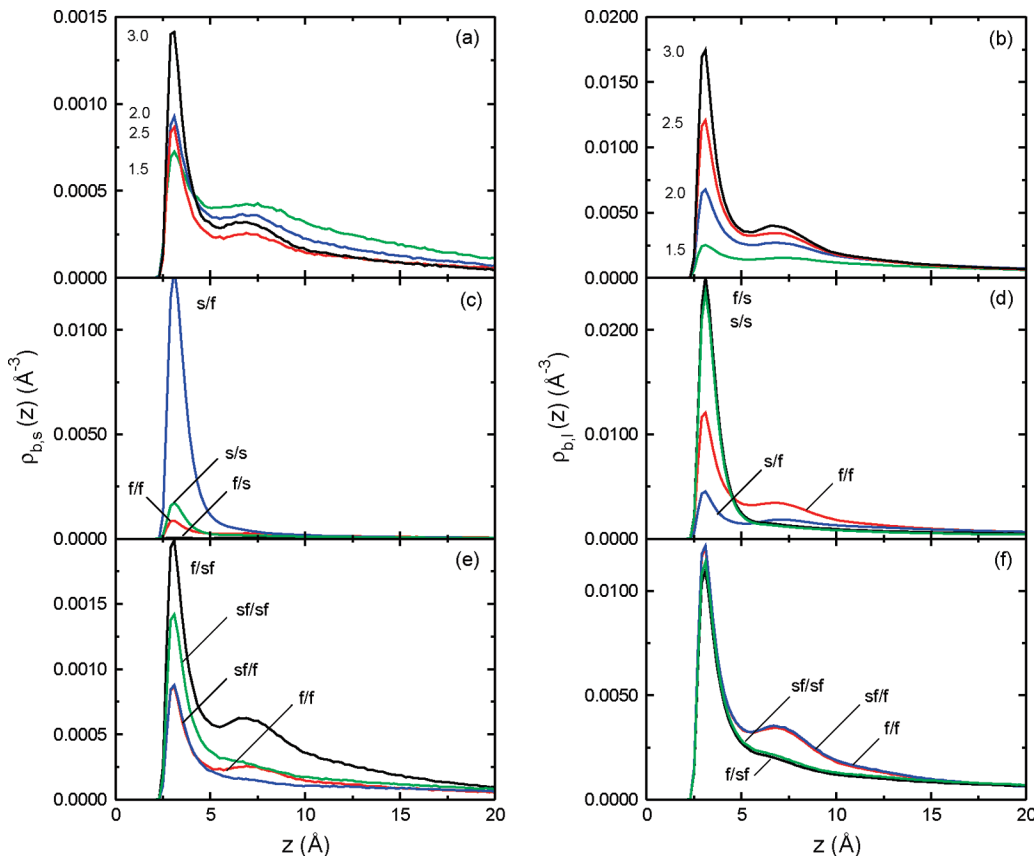


Figure 2. Bead density $\rho_{b,y}(z)$ as a function of the z -coordinate of the 20-mer (left column) and the 80-mer (right column) near a surface for systems belonging to (a and b) set I at the indicated value of ϵ_s in kJ/mol, (c and d) the f/f, s/f, f/s, and s/s systems belonging to set II, and (e and f) the f/f, sf/f, f/sf, and sf/sf systems belonging to set III.

beads of the 20-mer (filled circles) (i) are insensitive to the bead–surface interaction strength and (ii) are much smaller than the corresponding numbers in the absence of the longer 80-mer (open circles).

In more detail, the slope of $\langle N_{p,l}^{\text{ads}} \rangle$ and $\langle N_{b,l}^{\text{ads}} \rangle$ as a function of ϵ_s differs, indicating that the structure of adsorbed 80-mers depends on the bead–surface interaction strength. The relative expulsion of the 20-mer is smallest at $\epsilon_s = 1.5$ kJ/mol, where the adsorbed amount is small, but becomes larger at increasing bead–surface interaction strength. Furthermore, the growth of $\langle N_{p,s}^{\text{ads}} \rangle$ in the absence of the 80-mer starts to level off at $\epsilon_s = 2.5$ kJ/mol, the reason being that the bulk becomes depleted of the 20-mer (remember that $N_{p,s} = 94$).

Thus, for a one-component system, we find an increase in the number of adsorbed polymers and the number of adsorbed beads at increasing adsorption strength, whereas, in the bidisperse polymer system, the increase prevails for the 80-mer but the number of adsorbed polymers and the number of adsorbed beads of the 20-mer are essentially constant and smaller than those in the one-component system. Hence, we can already conclude that the different adsorption affinity due to different polymer lengths is sufficient to make (i) the adsorbed amount of the longer 80-mer essentially unaffected by the presence of the shorter 20-mer, (ii) the adsorbed amount of the shorter 20-mer strongly reduced but still nonzero, (iii) and the total amount of adsorbed beads of the 20-mer and 80-mer slightly larger than that for the 80-mer alone.

Moreover, an application of a lattice mean-field theory under as close conditions as possible gives results in excellent qualitative agreement with those presented here, suggesting that this theory is a useful complement to bead–spring models

solved by simulation techniques for examination of competitive adsorption of flexible polymers. For further details, see the Appendix.

The z -distribution of the bead density $\rho_{b,s}(z)$ and $\rho_{b,l}(z)$ for set I is displayed in Figure 2a and b, respectively. For all ϵ_s values, there is a prominent maximum at $z = z_{\min}$, which represents the adsorbed layer of beads in physical contact with the surface. Depending on the conditions, a second adsorption maximum appears at $z \approx z_{\min} + \sigma$.

The 80-mer displays only a weak adsorption layer at $\epsilon_s = 1.5$ kJ/mol. As ϵ_s is increased to 3.0 kJ/mol, its maximal density grows 7-fold and a second adsorption layer is developed. As for the 20-mer, its density distribution also changes at increasing bead–surface interaction strength but at a nearly constant number of adsorbed beads. At increasing ϵ_s , the primary maximum increases but less drastically. Furthermore, the region with an enhanced polymer density becomes narrower and its density depends nonmonotonically on ϵ_s , indicating an intricate dependence on the combined effect of the bead–surface interaction strength and the interaction with the varying amount of adsorbed 80-mer.

5.2. Sets II and III. The values of the number of adsorbed polymers and of the number of adsorbed beads for systems belonging to sets II and III are given in Figure 3 in a bar chart representation. The four systems composed of flexible and stiff polymers (set II) are grouped together, as well as those involving flexible and semiflexible polymers (set III).

When one of the polymer types is stiff, $\langle N_{p,y}^{\text{ads}} \rangle$, $\gamma = \{s, 1\}$, and $\langle N_{b,y}^{\text{ads}} \rangle$, $\gamma = \{s, 1\}$, of that polymer type *increase*, whereas for the other and flexible polymer type in the mixture these numbers *decrease*. The 20-mer displays the largest relative

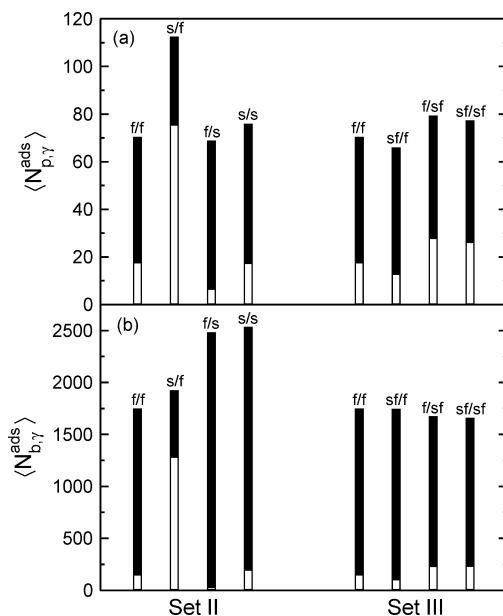


Figure 3. (a) Average number of adsorbed polymers ($\langle N_{p,\gamma}^{\text{ads}} \rangle$) and (b) average number of adsorbed beads ($\langle N_{b,\gamma}^{\text{ads}} \rangle$) of the 20-mer (open bars) and the 80-mer (filled bars) for systems belonging to sets II and III.

changes. With stiff 20-mer and flexible 80-mer (s/f system), $\langle N_{p,\gamma}^{\text{ads}} \rangle$ increases 4-fold (Figure 3a) and $\langle N_{b,\gamma}^{\text{ads}} \rangle$ increases 9-fold (Figure 3b). With flexible 20-mer and stiff 80-mer (f/s system), very few 20-mers remain adsorbed. When both polymer types are stiff (s/s system), the number of adsorbed polymers of the 80-mer displays a weak increase, whereas the number of adsorbed 80-mer beads increases by $\sim 45\%$ and adsorbed 20-mer beads by $\sim 30\%$. For the semiflexible polymers, the changes in $\langle N_{p,\gamma}^{\text{ads}} \rangle$, $\gamma = \{s, l\}$, and $\langle N_{b,\gamma}^{\text{ads}} \rangle$, $\gamma = \{s, l\}$, are much more subtle. Also, here the 20-mer displays the largest relative changes. However, here $\langle N_{p,\gamma}^{\text{ads}} \rangle$, $\gamma = \{s, l\}$, and $\langle N_{b,\gamma}^{\text{ads}} \rangle$, $\gamma = \{s, l\}$, decrease as the polymers become semiflexible and the corresponding values for the other polymer type increase. The adsorption data of the situation when both polymer types are semiflexible (sf/sf system) are close to that when only the 80-mer is semiflexible (f/sf system).

We will now continue to examine the bead density distribution for systems belonging to sets II and III. In our previous study,¹⁹ it was generally found that the first adsorption layer becomes more narrow and possesses a high density, whereas the second layer is suppressed and vanishes as the polymer becomes stiffer. Figure 2c–f shows that such an appearance also occurs in the mixed polymer solutions. For example, Figure 2d shows that the 80-mer displays only a single and enhanced first adsorption layer when it is stiff (f/s and s/s systems) and the appearance of two adsorption layers prevails when only the 80-mer remains flexible (f/f and s/f systems). A similar but less prominent tendency is found in Figure 2f, where the 80-mer is semiflexible. Furthermore, Figure 2e shows that the second adsorption layer of the 20-mer vanishes as the 20-mer is semiflexible with the flexible 80-mer (sf/f system) and Figure 2c displays that the same appears for the stiff 20-mer (s/f system), however, less clearly seen due to the extended vertical scale to encompass the large density variation of the adsorbed layers. Finally, Figure 2c shows that the density profile of the 20-mer is attenuated as the 80-mer becomes stiff (f/s system), whereas Figure 2e shows that this is enhanced as the 80-mer becomes semiflexible (f/sf system).

In summary, the adsorbed amount of beads of a polymer type (i) increases as the polymer becomes stiff but (ii) decreases

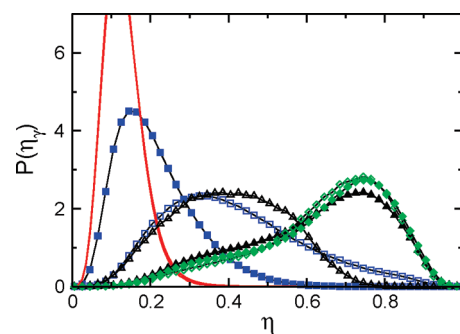


Figure 4. Normalized probability bond order distribution $P(\eta_\gamma)$ with domain radius $R_\eta = 20 \text{ \AA}$ of the 20-mer (open symbols) and the 80-mer (filled symbols) for the f/f (curves), s/f (squares), f/s (triangles), and s/s (diamonds) systems belonging to set II.

somewhat when it becomes semiflexible. These seemingly confound results can be rationalized from our previous investigation of the adsorption of 20-mers at a range of different flexibilities.¹⁹ There it was found that both $\langle N_p^{\text{ads}} \rangle$ and $\langle N_b^{\text{ads}} \rangle$ displayed extreme values near our semiflexible condition. A similar finding was earlier made by van Eijk and Leermakers for the adsorption of polymers at liquid–liquid interfaces using a lattice mean-field theory.²⁵ Observation (i) is connected to a strongly increased density of the first adsorption layer that exceeds the vanishing of the second adsorption layer (see Figure 2c and d). As for observation (ii), the second adsorption layer basically vanishes, but the density of the first adsorption layer remains essentially intact, leading to the smaller adsorbed amount. Furthermore, in the mixed solutions, the adsorbed amount of beads of the flexible polymer displays a variation which is the opposite to that of the semiflexible or stiff one. This can be viewed as a response to the increased or the reduced amount of surface space available to the flexible polymers. Thus, the bead density distribution profiles display systematic changes as one or both of the polymer types are made stiff or semiflexible and provide a background to the variation in the number of adsorbed beads at the various conditions.

We will now focus on the structure of the first adsorption layers as described by the nematic bond order analysis for systems belonging to set II. Figure 4 shows the probability bond order distribution $P(\eta)$ for the domain radius $R_\eta = 20 \text{ \AA}$. Data are given of the ordering of bonds belonging to different polymer types separately.

Data show that the probability distributions for the two polymer lengths of the reference system (curves) are basically the same and have a narrow peak at $\eta \approx 0.11$, indicating an essentially disordered orientation of bond directions. Furthermore, in the s/s system with both polymer types stiff, the bond orders of these are again very similar. However, the distribution is strongly shifted to larger values of η , demonstrating a pronounced nematic bond order. The properties of the systems with mixed flexibility display interesting features. In the s/f system with stiff 20-mer and flexible 80-mer, the ordering about bonds in the 20-mer (open squares) is enhanced, although not to the same extent as in the s/s system and the ordering about bonds in the 80-mer (open squares) is somewhat increased. However, in the f/s system with flexible 20-mer and stiff 80-mer, the ordering about bonds in the 20-mer (open triangles) is similar to that in the s/f system and the ordering about bonds in the 80-mer (filled triangles) is similar to that in the s/s system. Hence, with one polymer type being stiff, (i) the ordering about adsorbed bonds residing in both polymer types increases and (ii) the effect is much larger with stiff 80-mer than with stiff

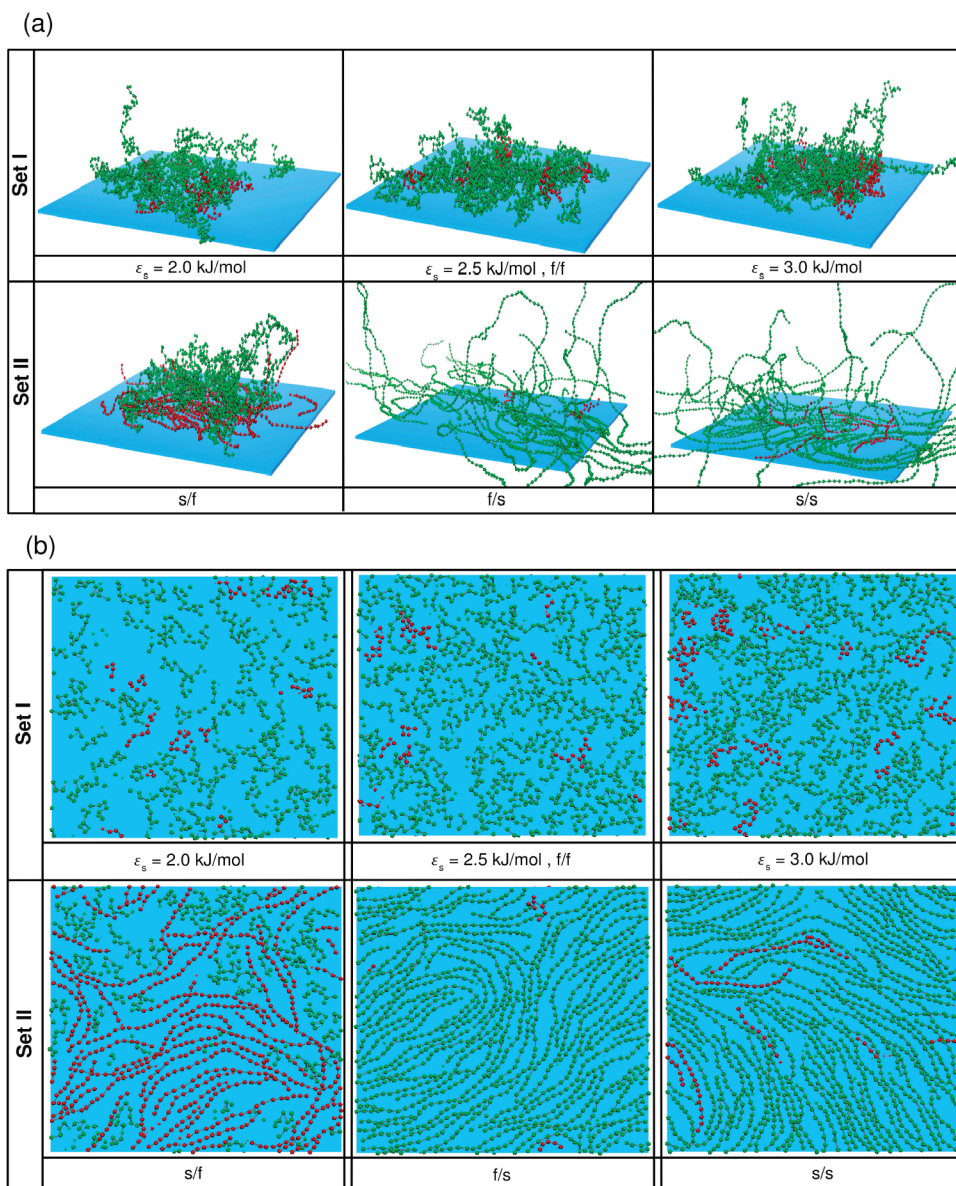


Figure 5. (a) Snapshots (perspective view) displaying one surface with adsorbed 20-mers (red) and 80-mers (green) and (b) snapshots (top view) displaying a surface with adsorbed beads of the 20-mer (red) and the 80-mer (green) for systems belonging to sets I and II taken from the end of the MC simulations. In part a, periodic boundary conditions have been suspended to illustrate the conformations of the adsorbed polymers and the plane (blue) is larger than the surface used in the simulations.

20-mer, which is most likely due to the larger number of beads residing in the 80-mer (Figure 3b).

5.3. Snapshots. Different snapshots taken from the end of the MC equilibrium simulations to illustrate different structural aspects comprising systems belonging to sets I and II are given in Figure 5, displaying adsorbed polymers (panel a) and adsorbed beads (panel b) at one surface.

In the snapshots given in Figure 5a, the periodic boundary conditions in the x - and y -directions have been removed to emphasize the conformation of adsorbed polymers and to better illustrate the orientation of the polymers with respect to the surface. Moreover, the side lengths of the adsorbing surface (blue planes) in the graphs are enlarged to $L_x = L_y = 300 \text{ \AA}$ (note $L_x = L_y = 200 \text{ \AA}$ in the simulations) to better accommodate the full length of the restored polymers. A drawback of this representation, however, is an impression of a less dense packing on the surface. In set I (top row), the increase of adsorbed 80-mers (green) and the unaltered number of adsorbed 20-mers (red) at increasing bead–surface interaction strength is faintly

visible. Also, systems with one or both polymer types being stiff are shown (bottom row). Obviously, the conformational differences between flexible and stiff chains are much larger than those appearing at increasing bead–surface interaction strength. In the s/f system, we see mainly flat conformations of the adsorbed 20-mers and predominantly perpendicularly oriented coiled 80-mers. In the f/s and s/s systems with stiff 80-mers, most of the adsorbed 80-mers are adsorbed parallel to the surface but with some chains stretching into the solution. In the f/s system, very few adsorbed flexible 20-mers are incorporated into this mesh, and in the s/s system, most of the adsorbed 20-mers are oriented parallel to the surface.

The snapshots in Figure 5b display one of the surfaces with adsorbed beads of the two polymer types to highlight the bond order at the surface. Set I (top row) encompasses systems with flexible polymers, and the snapshots support the notion that a higher bead–surface interaction strength results in a larger amount of adsorbed beads (see Figure 1b). Furthermore, we observe that a disordered structure is retained and that the

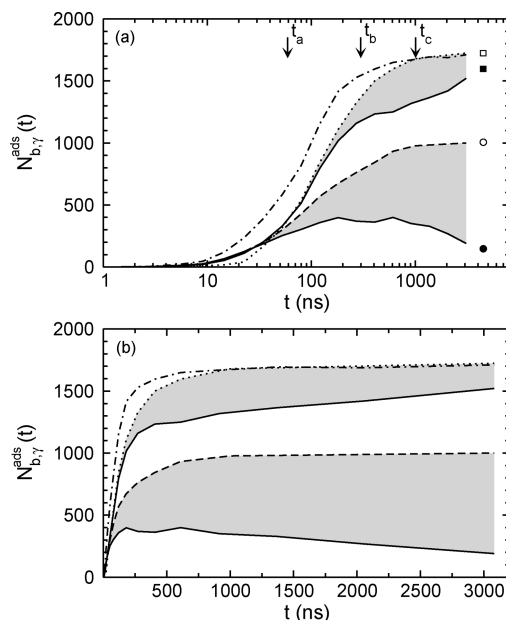


Figure 6. Number of adsorbed beads $N_{b,\gamma}^{\text{ads}}(t)$ using a (a) logarithmic and (b) linear abscissa scale as a function of time t of the 20-mer (lower solid curve) and the 80-mer (upper solid curve) of the reference system, their sum (dotted-dashed curve), as well as of the 20-mer (dashed curve) and the 80-mer (dotted curve) of monodisperse solutions. In part a, equilibrium data obtained by Monte Carlo simulations for the 20-mer (circles) and 80-mer (squares) for the reference (filled symbols) and monodisperse (open symbols) solutions are also given.

minority component is relatively well dispersed at all interaction strengths. Set II (bottom row and central top) involves mixed polymer solutions with different combinations of flexible and stiff polymers. First, we observe that adsorbed subchains of stiff 80-mers in the f/s and s/s systems become locally parallel, and that the order is not global in accordance with the bond order analysis (Figure 4). Furthermore, a comparison of the f/f and s/f systems confirms that a stiff 20-mer gives a larger amount of adsorbed 20-mer (Figure 3a) without a markedly enhanced bond order of the 80-mers as also previously concluded (Figure 4).

6. Adsorption Rates

In the following, we will examine the relaxation of the number of adsorbed beads $N_{b,\gamma}^{\text{ads}}(t)$, $\gamma = \{s, l\}$, from its zero value at the initial state, characterized by an ~ 20 Å thick polymer-free layer at the surfaces, toward its equilibrium $\langle N_{b,\gamma}^{\text{ads}} \rangle$, $\gamma = \{s, l\}$, as deduced from the BD simulations. This analysis will first be made in some detail for the reference system.

6.1. Reference System. The time dependence of the number of adsorbed beads of the 20-mer and the 80-mer of the reference system is displayed in Figure 6 on a logarithmic (panel a) and linear (panel b) abscissa scale. The former scale more advantageously describes the processes appearing at different time regimes, and the latter scale is more common when presenting experimental data. Figure 6 also shows the total number of adsorbed beads and the corresponding data from 20-mer and from 80-mer monodisperse solutions at the same 20-mer and 80-mer polymer density, respectively, as in the bidisperse system. The shaded area gives a visual representation of the reduced evolution of $N_{b,\gamma}^{\text{ads}}(t)$, $\gamma = \{s, l\}$, of the bidisperse system as compared to the two monodisperse solutions.

From Figure 6a, we conclude the following adsorption scenario of the bidisperse solution. (I) At short times, $t < t_a \approx 60$ ns, the

adsorption of the 20-mer and 80-mer follows closely the adsorption process of their monodisperse solutions. A weak tendency of an enhanced adsorption rate of the 80-mers is seen. Nevertheless, basically, the initial adsorptions of the two polymer types appear independently of each other. (II) At longer times, $t_a < t < t_b \approx 300$ ns, the adsorption of the 20-mer and 80-mer lags behind the adsorption in the monodisperse systems. At this stage, the polymers of the different types start to compete for space at the surface. It appears that the 20-mer is affected earlier and at a lower total bead concentration, which could be due to the weaker 20-mer–surface affinity due to its shorter polymer length. (III) At the time $t = t_b$, the adsorption of the 20-mer displays a maximum corresponding to half of the adsorbed amount in its monodisperse solution. Furthermore, at this stage, the adsorption of the 80-mer vs the logarithm of the time displays a kink, implicating an altered adsorption process as compared to its monodisperse solution. (IV) At $t_b < t < t_c \approx 1000$ ns, the 20-mer is competitively desorbed from the surface by the 80-mer, and the adsorption of the 80-mer is still hindered by the presence of the 20-mer at the surface. (V) After $t = t_c$, the total number of adsorbed beads has reached its equilibrium value, and thereafter, there is a slow exchange of 20-mers by 80-mers. (VI) At equilibrium (symbols), still some 20-mers remain adsorbed, and the adsorbed amount of 80-mers is $\sim 10\%$ smaller than in its monodisperse solution. Hence, the larger 80-mer–surface affinity as compared to the 20-mer–surface affinity does not totally eliminate an adsorption of 20-mers.

The ratio of the maximal amount of adsorbed 20-mers at $t = t_b$ and the equilibrium amount of 20-mers of the bidisperse system will be referred to as the degree of *overadsorption*. The occurrence of an overadsorption of a flexible polymer is here a consequence of (i) the faster diffusion and (ii) the weaker polymer–surface affinity of the 20-mer as compared to the 80-mer. For the reference system, the relative overadsorption is about three.

Finally, Figure 6b with a linear abscissa illustrates the relatively quick adsorption to $t \approx t_b$ and the much slower exchange dynamics appearing thereafter. The principal shape of the adsorption curves closely resembles those previously obtained from experiments by Fu and Santore⁷ and MC simulations by Jiang et al.¹⁴

6.2. Set I. Figure 7 shows the number of adsorbed beads $N_{b,\gamma}^{\text{ads}}(t)$, $\gamma = \{s, l\}$, as a function of time t for various ϵ_s values of systems belonging to set I. Generally, the adsorption of the 20-mer and the 80-mer increases at increasing bead–surface interaction strength. Such an increase of adsorbed 20-mer in monodisperse polymer solutions has been discussed earlier.¹⁹ Furthermore, both the appearance of (i) an adsorption maximum of the shorter 20-mer before reaching its equilibrium amount and (ii) a kink in the adsorption vs the logarithm of the time for the adsorption of the longer 80-mer remain at weaker and stronger bead–surface interaction. However, with increasing bead–surface interaction, (iii) the location of these features at $t = t_b$ shifts to shorter time (here from ~ 400 to 250 ns) and (iv) the degree of relative overadsorption of the short polymer increases.

Thus, also for a bidisperse polymer solution, the initial adsorption rate increases with bead–surface interaction strength. Furthermore, the preference of the longer 80-mer over the shorter 20-mer at increasing surface attraction makes the initial build-up of the short polymer and the subsequent removal of it more prominent.

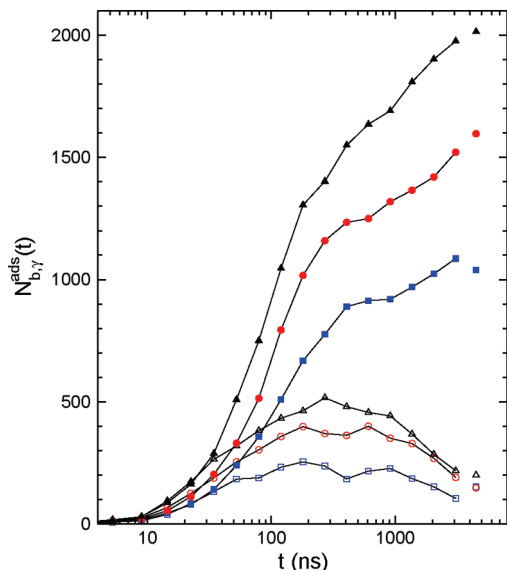


Figure 7. Number of adsorbed beads $N_{b,y}^{ads}(t)$ as a function of time t of the 20-mer (open symbols) and the 80-mer (filled symbols) for systems belonging to set I at $\epsilon_s = 2.0 \text{ kJ/mol}$ (squares), 2.5 kJ/mol (circles), and 3.0 kJ/mol (triangles). Equilibrium data (right edge) obtained by MC simulations are also given.

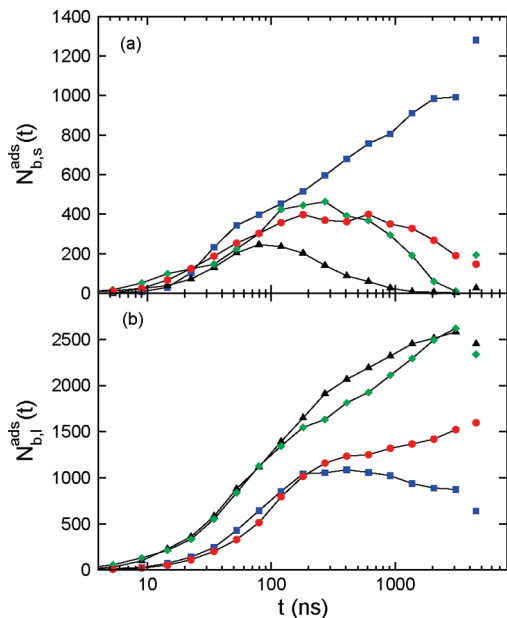


Figure 8. Number of adsorbed beads $N_{b,y}^{ads}(t)$ as a function of time t of (a) the 20-mer and (b) the 80-mer for the f/f (circles), s/f (squares), f/s (triangles), and s/s (diamonds) system belonging to set II. Equilibrium data (right edge) obtained by MC simulations are also given.

6.3. Set II. The number of adsorbed beads $N_{b,y}^{ads}(t)$, $y = \{s, l\}$, as a function of time t for systems belonging to set II are shown in Figure 8 for the 20-mer (panel a) and the 80-mer (panel b).

The behavior of the s/s system, where both polymer types are stiff, is similar to the reference (f/f) system already discussed. However, the 20-mer displays a more marked overadsorption and the adsorbed amount of the 80-mer is larger; both changes are in agreement with the inference that a stiff polymer displays a stronger surface affinity as compared to a flexible one. Thus, enhancing the surface affinity by either (i) increasing the bead–surface attraction or (ii) making both polymers simultaneously stiff has a similar effect on the dynamics of the number of adsorbed beads.

With either of the polymers stiff and the other flexible, substantial and interesting features appear. As for the s/f system, the adsorption of the stiff and shorter 20-mer increases monotonically, whereas the adsorption of the flexible and longer 80-mer displays a maximum before it decays to its equilibrium value. Thus, the stronger surface affinity of a stiff polymer as compared to a flexible one can more than compensate for the weaker surface affinity coming from a 4-fold shorter polymer length. Hence, we have the case where a short polymer may displace a longer one with the same polymer–surface intermolecular interactions.

For the f/s system, both the longer length and the larger stiffness of the 80-mer make the maximal adsorbed amount of the 20-mer smaller and appearing at shorter times. Furthermore, the equilibrium amount of the flexible 20-mer is very small, as already alluded to in Figure 3.

As a consequence of the low number of adsorbed beads at the end of the BD simulation for the 20-mer in the f/s and s/s systems where the 80-mer is stiff (Figure 8a), we choose to omit data points for $t > 1000 \text{ ns}$ in the analysis of the conformational dynamics in section 7.

We have previously shown that the time to achieve adsorption equilibrium for monodisperse solutions increases with increasing polymer stiffness.¹⁹ In the mixed solution, this is here manifested on some occasions where the adsorbed amounts at the end on the BD simulation and the MC simulations are less coherent for stiff polymers. For example, for the f/s system, a near agreement is found for both polymer lengths, whereas the adsorbed amounts of the s/f system at the end of the BD simulations have not reached the MC values and the BD data of the s/s system has passed the MC data, possibly indicating that the MC results here suffer from incomplete equilibration.

7. Conformational Dynamics

7.1. Set I. **7.1.1. Radius of Gyration.** The dynamics of the polymer extensions expressed by $\langle R_{g,y}^2(t) \rangle_{\perp}$ and $\langle R_{g,y}^2(t) \rangle_{\parallel}$ of the 20-mer and 80-mer have been examined in the bidisperse solution at various bead–surface interaction strengths. This dynamics does not differ strongly from that in corresponding monodisperse solutions. An account of these properties of the f/f system at $\epsilon_s = 2.5 \text{ kJ/mol}$ (the reference system) is given in subsection 7.2.1.

7.1.2. Tails, Loops, and Trains. Generally, the time development of tails, loops, and trains is close to that observed for flexible 20-mers in monodisperse solutions. Predominantly, beads are found in tails at an early stage of the adsorption; thereafter, the fraction of beads in tails is reduced and more beads are found in loops and trains. In the final relaxation phase, more beads are found in tails and less in trains; these changes are driven by repulsion between adsorbed polymers. The magnitude of the final relaxation phase increases with increasing bead–surface interaction strength.

The results given in Figure 9 show that basically the same behavior prevails in bidisperse solutions. In more detail, the conformational dynamics is faster for the 20-mer. The fraction of beads in tails displays a minimum of 20–30% (Figure 9a) and the fraction of beads in trains a maximum of 50–70% (Figure 9c) at $t \approx t_a$, the time at which the adsorption of the 20-mers starts to be affected by the presence of adsorbed 80-mers. The fraction of beads in loops increases with time and early reaches a plateau value of 20%, the value being independent of ϵ_s (Figure 9b). The final relaxation phase of the 80-mer starts at $t \approx t_b$, the time at which the total number of adsorbed beads is 90% of its maximal value; here, the fraction of beads

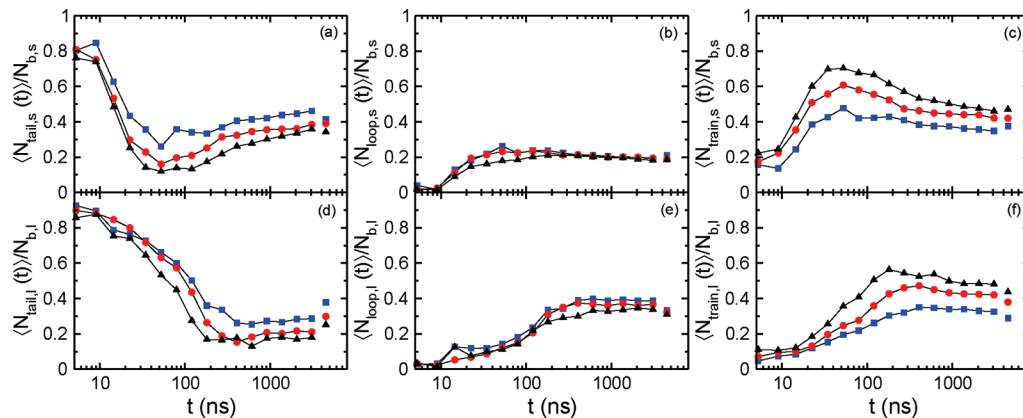


Figure 9. Average fraction of beads in (a and d) tails, (b and e) loops, and (c and f) trains $\langle N_{\alpha,\gamma}(t) \rangle / N_{b,\gamma}$, $\alpha = \{\text{tail, loop, train}\}$, as a function of time t of (a, b, and c) the 20-mer and (d, e, and f) the 80-mer for systems belonging to set I at $\varepsilon_s = 2.0$ kJ/mol (squares), 2.5 kJ/mol (circles), and 3.0 kJ/mol (triangles). Equilibrium data (right edge) obtained by MC simulations are also given.

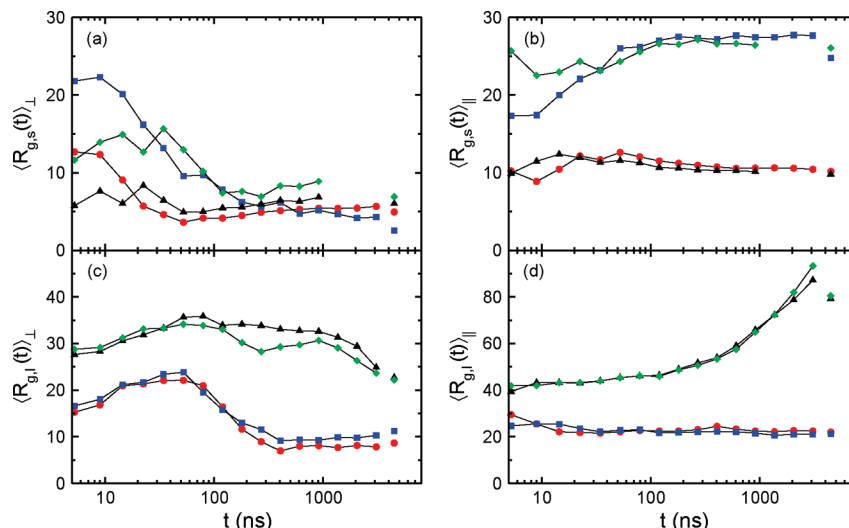


Figure 10. (a and c) Root-mean-square radius of gyration perpendicular to the adsorbing surface $\langle R_{g,s}^2(t) \rangle_{\perp}^{1/2}$ and (b and d) root-mean-square radius of gyration parallel to the adsorbing surface $\langle R_{g,l}^2(t) \rangle_{\parallel}^{1/2}$ as a function of time t of (a and b) the 20-mer and (c and d) the 80-mer for the f/f (circles), s/f (squares), f/s (triangles), and s/s (diamonds) system belonging to set II. Equilibrium data (right edge) obtained by MC simulations are also given.

of the 80-mer in tails possesses a weak minimum (Figure 9d) and in trains a weak maximum (Figure 9f). Finally, the fraction of 80-mer beads in loops also approaches a plateau at $t \approx t_b$ (Figure 9e). Noticeably, the fraction of beads in loops of the 80-mers is considerably larger than the corresponding fraction in the 20-mer.

7.2. Set II. 7.2.1. Radius of Gyration. Figure 10 displays the components of the radius of gyration as a function of time for the adsorbed 20-mers (top row) and 80-mers (bottom row) of the four mixed systems belonging to set II. The most apparent observation is that the perpendicular and parallel extension (i) of both flexible and stiff polymers and (ii) of both lengths display time dependence, which to a large degree is independent of the stiffness of the dissimilar polymer type. This observation is most marked for the parallel extension and for the 80-mer. For example, Figure 10d shows that the $\langle R_{g,l} \rangle_{\parallel}$ values of the f/f and s/f systems, where the 80-mer is flexible and the 20-mer is either flexible or stiff, nearly coincide, and the same is true for the f/s and s/s systems, where the 80-mer is stiff. Furthermore, the least accordance of this observation appears for the perpendicular extension of the 20-mer given in Figure 10a. One possible reason for the relatively large difference in $\langle R_{g,l}^2(t) \rangle_{\perp}^{1/2}$ of the 20-mer between the s/f and s/s systems, where the 20-mer is stiff, might be that the 20-mer is the surface majority component in the s/f system, whereas it is the surface minority component in the s/s

system. Nevertheless, we obtain the notion that the extension perpendicular and parallel to the surface of a polymer is basically insensitive to the stiffness of the other polymer type upon adsorption from a mixed solution.

Our second observation is that the relaxation to equilibrium is (i) faster for the 20-mer as compared to the 80-mer and (ii) faster for flexible as compared to stiff polymers. This is, e.g., illustrated by comparing $\langle R_{g,l}^2(t) \rangle_{\parallel}^{1/2}$ for the f/f system of the 20-mer (Figure 10a, red symbols) with that of the 80-mer (Figure 10c, red symbols), where approximately equilibrium values are achieved after 40 and 300 ns, respectively. Furthermore, the relaxation of stiff 80-mer appears first after a few 1000 ns (Figure 10c and d, black and green symbols); apparently, a few adsorbed stiff 80-mers become end-adsorbed at late stage (see Figure 5a, f/s and s/s systems), making room for additional polymers to become adsorbed.

The seemingly large difference in the final relaxation of $\langle R_{g,l}^2(t) \rangle_{\perp}^{1/2}$ and $\langle R_{g,l}^2(t) \rangle_{\parallel}^{1/2}$ between flexible and stiff polymers is a result of different structural rearrangements; for flexible polymers, it involves a final reduction of the area per polymer arising from the polymer–polymer repulsion and for stiff polymers a packing and forming of an ordered polymer layer at the surface.¹⁹

7.2.2. Tails, Loops, and Trains. The average fraction of beads in tails, loops, and trains as a function of time for adsorbed

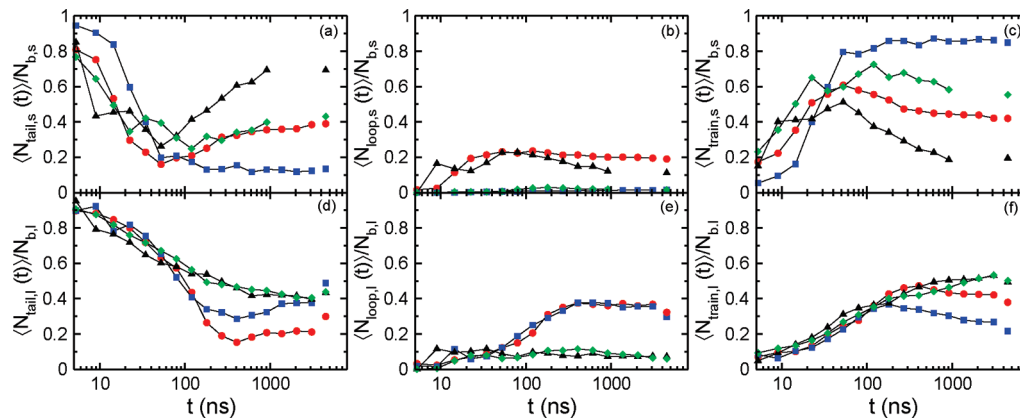


Figure 11. Average fraction of beads comprising (a and d) tails, (b and e) loops, and (c and f) trains $\langle N_{\alpha,y}(t) \rangle / N_{b,y}$, $\alpha = \{\text{tail}, \text{loop}, \text{train}\}$, as a function of time t of (a, b, and c) the 20-mer and (d, e, and f) the 80-mer for the f/f (circles), s/f (squares), f/s (triangles), and s/s (diamonds) system belonging to set II. Equilibrium data (right edge) obtained by MC simulations are also given.

20-mers (top row) and 80-mers (bottom row) of the four mixed systems belonging to set II is given in Figure 11. As for the polymer extension, there is an underlying difference of the tail, loop, and train characteristics between flexible and stiff chains. Whereas the extension of adsorbed polymers is insensitive to the degree of flexibility of the *other* polymer type in a mixed solution, we will see that this is generally not true for the fraction of beads in the three types of subchains.

Our first observation is that the fractions of *tails* and *trains* are (in most cases) *dependent* of the stiffness of the *other* polymer type, whereas the fractions of beads in *loops* for both flexible and stiff polymers of both lengths display time dependencies that are essentially *independent* of the stiffness of the *other* polymer type.

Specifically, the fraction of beads in tails of (i) flexible 20-mer, (ii) stiff 20-mer, and (iii) flexible 80-mer is increased as the other polymer in the mixed solution is changed from a flexible to a stiff polymer, and consequently, the fraction of beads in trains for the same change is reduced. However, the fraction of beads in trains and tails of stiff 80-mers develops independently of the stiffness of the 20-mer. The difference in the fraction of beads in tails and trains develops generally first after ~ 100 ns. For example, if focusing on trains, Figure 11c shows that the fraction of beads in trains of the flexible 20-mer becomes smaller in the f/s system with the stiff 80-mer (black triangles), as compared in the f/f system with the flexible 80-mer (red circles). Similarly, Figure 11c also shows that the fraction of beads in trains of the stiff 20-mer in the s/s system (green diamonds) is smaller than that in the s/f system (blue squares). Furthermore, Figure 11f displays that the fraction of beads in trains of flexible 80-mers in the s/f system with the stiff 20-mer (blue squares) is smaller than in the f/f system with the flexible 20-mer (red circles). Finally, by monitoring Figures 11a and b, similar conclusions can be made for the fraction of beads in tails.

We have previously found that, in most cases, a polymer gains surface affinity (Figures 3 and 8) and adsorbs in flatter configuration (Figure 5b) at increasing stiffness. Thus, we conclude that this increase of adsorbed amount and flatter configuration indirectly may affect the tail and train characteristics of the other polymer adsorbed from a mixed polymer solution. We anticipate that the exception, which appeared for the stiff 80-mer, is that the surface affinity between a stiff 80-mer and a 20-mer, independent of its stiffness, is so large that the configuration of the stiff 80-mer remains unaffected. This is in accordance with the observation that the growth of the

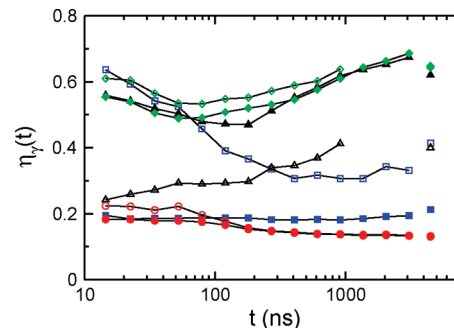


Figure 12. Bond order $\eta_\gamma(t)$ as a function of time t for the domain radius $R_\gamma = 20$ Å of the 20-mer (open symbols) and the 80-mer (filled symbols) for the f/f (circles), s/f (squares), f/s (triangles), and s/s (diamonds) system belonging to set II. Equilibrium data (right edge) obtained by MC simulations are also given.

number of adsorbed beads of the stiff 80-mer is insensitive to the stiffness of the 20-mer (Figure 8b). In summary, when the adsorption affinity increases for one of the polymer types in a mixed polymer solution and where the adsorption affinity of the two polymer types is not too dissimilar, the anchoring of the other polymer becomes poorer and the fraction of its beads residing in tails increases. This influence of the adsorption state of the other polymer appears to become prominent first at $t \approx t_b$, where the surface minority component displays its adsorption maximum (Figure 6a).

As for the relaxation of the polymer extensions, the relaxation of beads in various subchains is (i) faster for the 20-mer as compared to the 80-mer and (ii) faster for flexible as compared to stiff polymers. This is, e.g., illustrated by comparing $\langle N_{\text{train},y}(t) \rangle / N_{b,y}$ for the f/f system of the 20-mer (Figure 11c, red symbols) with that of the 80-mer (Figure 11f, red symbols), where near equilibrium values are achieved after 300 and 1000 ns, respectively. Furthermore, the relaxation of the stiff 80-mer appears first after a few 1000 ns (Figure 11d and e, black and green symbols).

7.2.3. Nematic Bond Order. The time evolution of the local nematic bond order for systems belonging to set II are given in Figure 12 for the domain radius $R_\gamma = 20$ Å. As previously, separate analysis of the two polymer types was made. The time window begins at 10 ns, at which a few polymers have adsorbed (Figure 8).

In Figure 12, we find that at $t = 10$ ns, η clusters around 0.2 for flexible polymers and around 0.6 for the stiff polymers. At these early stages with just a few polymers adsorbed, the contribution to the bond order comes mainly from intrachain

bond pairs. Hence, we conclude that polymers are sufficiently separated not to mutually affect the local bond order at this stage of the adsorption process. As for the f/f system, where both the 20-mer and the 80-mer are flexible, the bond order of these polymers starts at ~ 0.2 and decreases to ~ 0.15 during the adsorption process (cf. the final conformation of adsorbed bonds in the top center panel of Figure 5b). Considering the s/s system, where both polymer types are stiff, the evolutions of their bond orders are very similar to each other with a slightly larger bond order for the shorter 20-mer. The bond order decreases initially, displaying a minimum, and then grows slowly with time, which is the same appearance as in a monodisperse polymer solution (cf. Figure 12b of ref 19).

Turning again to the systems with polymers of mixed stiffness, the bond order of the flexible 80-mer in the s/f (filled squares) system remains constant at ~ 0.2 , and thus ends slightly larger in the presence of a stiff 20-mer as compared to a flexible 20-mer. More drastically is the large reduction of the bond order of the stiff 20-mer in the s/f (open squares) system from 0.6 to 0.35. Although the number of adsorbed beads of the 20-mer exceeds those of the 80-mer, the dispersely adsorbed coils of 80-mers obviously reduces the tendency of a nematic ordering of the 20-mer. This type of arrangement is clearly seen in the upper part of the lower left panel in Figure 5b. At last, the dynamics of the bond order of the stiff 80-mer in the f/s (filled triangle) system is close to that of the 80-mer in the s/s (filled diamond) system. However, the flexible 20-mer in the f/s (open triangle) system displays a progressively increased bond order during the adsorption. Hence, as the 20-mers are very few in this system, probably we mostly observe the induced straightening of individual polymers in the matrix of locally ordered 80-mers (see lower center panel of Figure 5b).

In summary: (i) In a mixed polymer solution with the short and long polymers having the same flexibility (flexible or stiff), the bond order of the two polymer types develops similarly. (ii) The bond order of stiff 20-mers in a mixed solution of stiff 20-mer and flexible 80-mer tends at equilibrium to adopt a low bond order. The influence of the stiff 20-mer on the bond order of the 80-mer is weak. (iii) The bond order of flexible 20-mers in a mixed solution of flexible 20-mer and stiff 80-mer tends at equilibrium to adopt a high bond order. The influence of flexible 20-mer on the bond order of the 80-mer is negligible.

8. Discussion

Fu and Santore⁷ measured competitive adsorption of bidisperse PEO [poly(ethylene oxide)] from aqueous solution onto silica using a mass ratio between 3 and 4, similar to the ratio used in our study. They nicely showed, by combined fluorescence and reflectivity techniques, that they could separate the time dependence of the adsorption for the individual polymer components. In their system containing PEO molecular weights of 33 000/120 000 (Figure 3 of ref 7), they concluded on the basis of a linear dependence of the adsorbed amount that the entire adsorption and desorption process of the smaller PEO was diffusion controlled. However, for the pairs 120 000/460 000 and 120 000/963 000 (Figure 8 of ref 7), the desorption of the smaller PEO became much slower than expected from a diffusion model. Furthermore, at most, only a reminiscence of an adsorption plateau appearing in the fully diffusion controlled case remained.

We have previously concluded¹⁹ that, beside the very initial adsorption, the adsorption process in our setup is slower than diffusion-limited. The appearance of a slow exchange process and essentially no adsorption plateau found by Fu and Santore

in some of their experiments concur with the observation in our simulation study. We thus argue that this supports the notion that the exchange process is kinetically controlled in these experiments as well as in our simulation study. Finally, we recognize that the length and time scales involved in the experiments and our simulations are vastly different. Nevertheless, we still believe that the fundamental processes involved are closely related.

9. Summary and Outlook

The competitive adsorption from mixtures of uncharged homopolymers of varying contour length onto planar surfaces in good solvent has been investigated. The effect of polymer–surface interaction strength and different combinations of stiffness between the polymer types were studied. Monte Carlo simulations were used to examine equilibrium properties of final adsorbed structures. The dynamics of the adsorption process was realized through Brownian dynamic simulation techniques.

For bidisperse flexible polymer solutions with a polymer length ratio of 4, we find a general adsorption behavior where we identified a number of characteristic features. Specifically, three points in time were extracted which mark the appearance of (i) a deviation of the adsorbed number of beads as compared to the related monodisperse solutions with the reduction being much more pronounced for the shorter polymer, (ii) a maximal number of adsorbed beads of the shorter polymer which is reached at the same time as the adsorption of beads from the longer polymer, revealing a significant decrease of the growth rate, and (iii) a slow exchange of shorter polymers for longer ones at a constant number of beads at the surface. Furthermore, at increasing bead–surface interaction strength, the maximal overadsorption of beads of the short polymer appears at shorter times and becomes more pronounced.

For mixtures containing combinations of stiff and flexible polymers of either polymer length, we find in particular (i) that stiff and long polymers fully dictate the adsorption behavior in terms of the number of adsorbed beads and bond order at the surface and (ii) an overadsorption of long and flexible polymers in the presence of short and stiff polymers, i.e., the stiff and short polymers replace the long and flexible polymers at the surface. The structure of the adsorbed layer shows that the fractions of polymers in tails and trains are largely dependent upon the stiffness of the dissimilar polymer type in the mixture.

Possible future investigations may comprise systems with a more complex distribution of polymer lengths. This could resolve effects of polydispersity on competitive adsorption, a situation which is often presented in experimental situations or applications. Moreover, comparison with scaling predictions such as those presented by Baschnagel et al.¹⁵ would be very valuable. However, first theory and simulation have to cover the same concentration and interaction regimes.

Acknowledgment. The authors thank Center for Scientific and Technical Computing at Lund University (LUNARC) for generous allocation of computer resources. Financial support by the Swedish Research Council (VR) is also gratefully acknowledged.

Appendix

Static equilibrium properties of the adsorption of polymers on a solid surface have been modeled by using a lattice mean-field theory. The theory used was initially developed for adsorption of uncharged homopolymers on planar surfaces by Scheutjens and Fleer²⁶ and has later been extended extensively.^{2,27}

In this appendix, we (i) briefly introduce this theory, (ii) assign values to parameters to describe competitive adsorption under conditions as close as possible to our bead–spring model, and (iii) provide results on the adsorbed amount under competitive conditions.

The lattice mean-field theory is characterized by dividing the space adjacent to a planar surface into layers and each layer is further divided into lattice cells of equal size. Within each layer, the Bragg–Williams approximation of random mixing is applied, and thus all lattice cells in a layer are equivalent. A lattice cell contains either a polymer segment or solvent. Interactions are short-ranged and are described by Flory–Huggins χ -parameters. The interaction of the molecules in the solution with a surface is described similarly. The numerical solution of the model invokes the determination of statistical weights of all possible polymer conformations consistent with the external conditions, from which properties such as volume fraction profiles, adsorbed amount, and loop, tail, and train characteristics can be extracted.

As for parameter assignment, we equated one segment with a bead of the bead–spring model; hence, polymers with 20 and 80 segments were modeled. Furthermore, we have adopted the athermal condition $\chi_{\text{polymer,solvent}} = 0$, which closely matches the truncated and shifted bead–bead LJ potential. Negative differences between the polymer–surface and solvent–surface interaction parameters ($\chi_{\text{polymer,surface}} - \chi_{\text{solvent,surface}} < 0$) were selected to match the attractive bead–surface potential described by ε_s . Since $\chi_{\text{polymer,surface}} - \chi_{\text{solvent,surface}}$ and ε_s describe interactions in different models, an exact numerical matching of these variables is not possible. Moreover, in the lattice theory, the excess adsorbed amount Γ_{exe} denotes the excess adsorbed polymer in an equivalent number of adsorbed layers. If we assign the cross-sectional area $\langle R_{bb}^2 \rangle$ to each bead in the bead–spring model, we have $\Gamma_{\text{exe},y} \approx \langle N_{b,y}^{\text{ads}} \rangle \langle R_{bb}^2 \rangle / (2L_x L_y)$. For example, here $\langle N_{b,y}^{\text{ads}} \rangle = 2000$ would correspond to $\Gamma_{\text{exe},y} \approx 0.8$.

Figure 13 displays the excess adsorbed amount $\Gamma_{\text{exe},y}$ as a function of $-RT(\chi_{\text{polymer,surface}} - \chi_{\text{solvent,surface}})$ of 80-mers (filled squares) and 20-mers (filled circles) of a solution composed of 80-mers, 20-mers, and solvent at the volume fractions $\phi_l = 0.01$ and $\phi_s = 0.01$; of 80-mers (open squares) of a solution composed of 80-mers and solvent at $\phi_l = 0.01$; and of 20-mers (open circles) of a solution composed of 20-mers and solvent at $\phi_s = 0.01$.

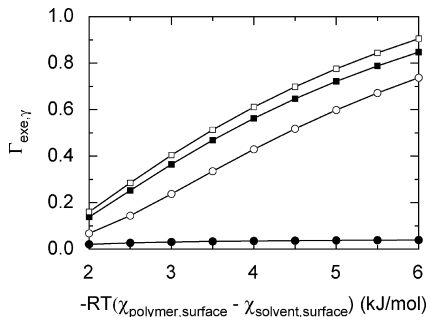


Figure 13. Excess adsorbed amount $\Gamma_{\text{exe},y}$ as a function of the effective polymer–surface attraction $-RT(\chi_{\text{polymer,surface}} - \chi_{\text{solvent,surface}})$ of the 80-mer (filled squares) and the 20-mer (filled circles) from a solution composed of 80-mers, 20-mers, and solvent at the volume fractions $\phi_l = 0.01$ and $\phi_s = 0.01$; of the 80-mer (open squares) of a solution composed of 80-mers and solvent at $\phi_l = 0.01$; and of the 20-mer (open circles) of a solution composed of 20-mers and solvent at $\phi_s = 0.01$ at athermal solution conditions and $T = 298$ K as predicted from lattice mean-field theory.

(circles) of a solution composed of 20-mers and solvent at $\phi_s = 0.01$. A comparison of the results of the lattice mean-field model given in Figure 13 with those of the coarse-grained bead–spring model given in Figure 1b shows that, notwithstanding the approximate transformations of values of variables between the two models, the ranges of the predicted adsorbed amount are similar for the two models. Furthermore, a closer comparison shows that the lattice mean-field model reproduces a number of salient features given in Figure 1b. In particular, we notice that (i) the adsorption of the 80-mer in the mixed solution increases with increasing polymer–surface attraction, (ii) the adsorption of the longer 80-mer in the mixed solution is close but slightly smaller than that of 80-mers from a pure 80-mer solution, (iii) the adsorption of the shorter 20-mer from the mixed solution is low and constant, and (iv) the adsorption of the shorter 20-mer from the mixed solution is much lower than from a pure 20-mer solution and the difference increases with increasing polymer–surface attraction.

Thus, our comparison suggests the lattice mean-field theory to be useful to examine static properties such as adsorbed amount under competitive conditions. In passing, we notice that the computational effort of solving the bead–spring model by the MC simulation and solving the lattice mean-field theory differs by 4–5 orders of magnitude. Moreover, this ratio increases with polymer length.

References and Notes

- (1) Fleer, G. J.; Lyklema, J. *Adsorption From Solution at the Solid/Liquid interface*; Academic Press: New York, 1983.
- (2) Fleer, G. J.; Cohen Stuart, M. A.; Scheutjens, J. H. M. H.; Cosgrove, T.; Vincent, B. *Polymers at interfaces*; Chapman & Hall: London, 1993.
- (3) Evans, D. F.; Wennerström, H. *The Colloidal Domain: Where Physics, Chemistry, Biology and Technology Meet*, 2nd ed.; Wiley-VCH: New York, 1999.
- (4) Dijt, J. C.; Cohen Stuart, M. A.; Fleer, G. J. *Macromolecules* **1994**, 27, 3219.
- (5) Santore, M.; Fu, Z. *Macromolecules* **1997**, 30, 8516.
- (6) Krabi, A.; Cohen Stuart, M. A. *Macromolecules* **1998**, 31, 1285.
- (7) Fu, Z.; Santore, M. *Macromolecules* **1998**, 31, 7014.
- (8) Chornatay, V. N.; Todosiichuk, T. T.; Menzheres, G. Ya.; Lipatov, Yu. S.; Maslak, Yu. V. *Colloids Surf., A* **2008**, 318, 53.
- (9) Postmus, B. R.; Leermakers, F. A. M.; Koopal, L. K.; Cohen Stuart, M. A. *Langmuir* **2007**, 23, 5532.
- (10) Lipatov, Yu. S.; Dudarenko, G. V.; Chornaya, V. N.; Todosiichuk, T. T. *Colloids Surf., A* **2008**, 326, 53.
- (11) Daoud, M. *Macromolecules* **1991**, 24, 6748.
- (12) Fleer, G. J. *Colloids Surf., A* **1995**, 104, 271.
- (13) Devotta, I.; Mashelkar, R. A. *Chem. Eng. Sci.* **1996**, 51, 561.
- (14) Jiang, J.; Liu, H.; Hu, Y. *Macromol. Theory Simul.* **1998**, 7, 113.
- (15) Baschnagel, J.; Johner, A.; Joanny, J.-F. *Eur. Phys. J. B* **1998**, 6, 45.
- (16) Postmus, B. R.; Leermakers, F. A. M.; Cohen Stuart, M. A. *Langmuir* **2008**, 24, 6712.
- (17) Källrot, N.; Linse, P. *Macromolecules* **2007**, 40, 4669.
- (18) Källrot, N.; Dahlqvist, M.; Linse, P. *Macromolecules* **2009**, 42, 3641.
- (19) Linse, P.; Källrot, N. *Macromolecules* **2010**, 43, 2054.
- (20) Baschnagel, J.; Mayer, H.; Varnik, F.; Metzger, S.; Aichele, M.; Müller, M.; Binder, K. *Interface Sci.* **2003**, 11, 159.
- (21) Akinchina, A.; Linse, P. *Macromolecules* **2002**, 35, 5183.
- (22) Ermak, D. L.; McCammon, J. A. *J. Chem. Phys.* **1978**, 69, 1352.
- (23) Allen, M. P.; Tildesley, D. J. *Computer Simulations of Liquids*; Oxford University Press: Oxford, England, 1987.
- (24) Linse, P. *MOLSIM*, version 4.7; Lund University: Lund, Sweden, 2009.
- (25) van Eijk, M. C. P.; Leermakers, F. A. M. *J. Chem. Phys.* **1998**, 109, 4592.
- (26) Scheutjens, J. M. H. M.; Fleer, G. J. *J. Phys. Chem.* **1979**, 83, 1619.
- (27) Linse, P.; Björling, M. *Macromolecules* **1991**, 24, 6700.